# How intramolecular vibrational energy transport changes with rigidity and polarity of the environment?

Natalia I. Rubtsova, Zhiwei Lin, Robert T. Mackin, Igor V. Rubtsov\*

Department of Chemistry, Tulane University, New Orleans, Louisiana 70118, United States \*corresponding author: irubtsov@tulane.edu

Abstract. Vibrational energy transport through oligomeric polyethylene glycol (PEG) chains can occur ballistically via optical vibrational chain bands, showing fast and constant transport speed and high efficiency of the transport, thus offering means to transfer significant quanta of energy, exceeding 1000 cm<sup>-1</sup>, to large distances exceeding 60 Å. We report how the intramolecular energy transport time, throughchain transport speed, and end-group cooling rate depend on the rigidity and polarity of the environment. The experiments were performed with end-group labeled PEG oligomers using two-dimensional infrared (2DIR) spectroscopy. The ballistic energy transport was initiated at one end of the chain by exciting an azido moiety at ca. 2100 cm<sup>-1</sup> and recorded at another end of the chain by probing the carbonyl stretching mode of succinimide ester. We found that the rigidity of the environment, polystyrene (PS) matrix vs. a solution of similar polarity, did not change much the energy transport times, nor the through-chain transport speed. These results suggest that in mildly polar media, dynamic fluctuations, occurring in solution but largely frozen in a solid matrix, are not the dominant cause of the dephasing of the chain states, despite the presence of fast relaxation components in the solution. The similarity of the transport times in different media suggests that the secondary chain structure does not affect much the transport in PEG chains. The solvent polarity affected the intramolecular transport significantly: the transport efficiency in polar DMSO is ca. 1.6 fold smaller than that in nonpolar CCl<sub>4</sub> or PS. The cooling time of the succinimide ester end group is reduced in more polar solvents affecting the waiting time dependence shape and thus the energy arrival time to the reporter. The analysis of different ways of extracting the energy arrival time from the data is presented. The observed dependences of the through-chain transport time on the solvent polarity suggests the presence of more than one wavepacket propagating in the PEG chain with different group velocities.

#### 1. Introduction.

The vibrational energy transfer process in molecular systems is important for a wide range of fields, spanning from chemistry and biochemistry, to molecular electronics and novel materials. Understanding vibrational energy transport in molecules is one of the challenges of physical chemistry. 1-2 Molecules interact with the medium they are placed in and exchange energy with the medium. However, this interaction is orders of magnitude weaker than the strength of covalent bonds between atoms in typical organic molecules, resulting in a peculiar situation where the high-frequency modes of molecules became isolated from high-frequency modes of the medium and the energy exchange occurs predominantly through low-frequency modes. The isolation of the high-frequency modes in molecules from the environment, results, essentially, in trapping vibrational energy in high-frequency modes of the solute, which brings an additional opportunity of arranging ballistic vibrational energy transport in molecules via high-frequency modes, which can be fast and efficient. Vibrational mode delocalization is required for ballistic transport so oligomeric structures are the most suitable for such regime.

In the 1970s, Davydov proposed that vibrational energy can propagate ballistically via high-frequency modes of a protein backbone;<sup>3</sup> such transport has yet been observed to only a short distances.<sup>4</sup> Troe and coworkers reported that the energy transport via short alkane chains terminated with large organic moieties occurs ballistically through the chain in response to electronic excitation of one of

the end groups. 5-6 Ballistic signaling via long alkane chains was observed by Dlott and coworkers in selfassembled monolayers of alkylthiolates adsorbed at a gold surface.7 With the development of twodimensional infrared (2DIR) spectroscopy, 8-9 it became possible to access energy transport dynamics in molecules.<sup>4, 10-13</sup> Rubtsov and coworkers observed ballistic transport in a series of studies using dualfrequency 2DIR 14 and relaxation-assisted 2DIR (RA 2DIR)15 spectroscopies. In these studies, a vibrational tag and vibrational reporter were attached to different ends of an oligomeric chain. Vibrational excitation of the tag and its relaxation initiated a vibrational wavepacket in the chain; the arrival of the wavepacket to the other end of the chain was recorded via RA 2DIR by a frequency shift of the reporter mode. Ballistic transport via high-frequency optical bands of the chain was found in a variety of chains, including PEG (speed of ca. 5.5 Å/ps), 16-17 perfluoro alkane (3.9 Å/ps), 18-19 and alkane chains. 20 It was shown that the transport speed via alkane chains depends on the way the energy is introduced into the chain, and can vary from 14.4 Å/ps with an azido moiety tag,20 to 8.0 Å/ps with a C=O tag,21 and to 4.2 Å/ps with an amide I mode tag.<sup>22</sup> The chain bands transferring energy in each case of initiation were identified.<sup>23</sup> Theoretical approaches were developed to describe diffusive, ballistic, and directed diffusive transport mechanisms in molecules. 23-32 The RA 2DIR studies showed that the transport in non-oligomeric compounds is slow, featuring effective speed of ca. 1.5 Å/ps,33 and follows the directed diffusion mechanism.26

A vibrational wavepacket, a coherent superposition of the delocalized chain states, propagates in the chain and is prone to dephasing, which destroys its motion thus affecting the amount of energy delivered to the chain end group. Thermal fluctuations of the chain structure (inhomogeneity) and thermal fluctuations of the populations of the low-frequency modes of the oligomer induce dephasing of the chain states. In addition, fluctuations of the surroundings also induce chain-state dephasing. To identify the role of the dynamic solvent fluctuations in chain states dephasing, we investigated the intramolecular energy transport via PEG chains embedded into a polystyrene matrix and compared it with the transport in solution. The experiments in solution of different polarity were performed to understand the extent to which polar solvents affect the energy transport and dissipation.

## 2. Experimental Details

#### 2.1. Dual-frequency 2DIR and relaxation-assisted 2DIR measurements.

A fully-automated dual-frequency two-dimensional infrared (2DIR) three-beam spectrometer with heterodyned detection is described in detail elsewhere. 34-35 It uses a Ti:Sapphire laser (Libra, Coherent), producing 1.5 W power at 1 kHz repetition rate with 80 fs pulse duration at 806 nm. Pumped by the 806 nm beam, mid-IR pulses of ca. 120 fs duration are generated using two independently tunable optical parametric amplifiers and difference frequency generation units (Palitra-Duo, Quantronix). Two pairs of mid-IR pulses are generated - three of them interact with the sample in a non-collinear fashion, while one is used as a local oscillator (LO) for heterodyne detection of the 3<sup>rd</sup>-order field radiated by the sample (Fig. 1A). Co-propagating 3<sup>rd</sup>-order signal and the LO are dispersed in a spectrograph and detected with an array detector (MCT, 64 elements, Infrared Associates). The time delay between the first two laser pulses interacting with the sample, τ, was scanned and the data measured by the array detector were Fourier transformed to form  $\omega_{\tau}$  ordinate axis. The abscissa,  $\omega_t$  is obtained directly from the wavelength at the array detector. 2DIR spectra were measured at various waiting times, T, which is the time delay between the second and third laser pulses interacting with the sample. The molecular system is in a population state during T, while in coherence states during  $\tau$  and the observation time,  $t^{.9, 14, 36}$  RA 2DIR traces were obtained by scanning the waiting time up to 120 ps. One dimensional waiting-time kinetics traces are generated for each cross peak by integrating the 2DIR spectrum in the region around the peak.

**2.2. Preparation of optical quality polystyrene films and solution samples.** Polystyrene (PS) films of high optical quality with embedded guest molecules were prepared using PS of an average molecular

weight of 35000 g/mol and density of 1.06 g/ml at 25°C (331651, Aldrich). The preparation method involved pressing the tablets of PS with embedded molecules, which we optimized to obtain PS films of optical quality. Innear and nonlinear IR measurements were performed with 50-100  $\mu$ m thick standing-alone polystyrene films. The end-labeled az PEGn compounds (Fig. 1A) were purchased from Quanta BioDesign, Ltd. and used as received. The number of repeating PEG units, n, was 0, 4, 8, and 12. Note that az PEG0 contains just three methylene groups in its chain. The compounds feature an azido moiety at one chain end and succinimide ester at another end (Fig. 1A). The concentration of the guest compounds in the film was ca. 20 mM; the optical density of the main carbonyl peak of succinimide ester was ca. 0.4. IR experiments with solution samples were performed in a sample cell made of two 1-mm thick CaF2 wafers and a 50  $\mu$ m thick Teflon spacer.

**2.3. DFT Calculations.** DFT structure calculations were performed for the azPEG*n* compounds in vacuum, using a B3LYB functional and 6-311G++(d,p) basis set in a Gaussian-09 suite. The throughbond distances were obtained as a summation of all bond lengths on the path. Note, that the throughbond distances are independent on the structural distribution of flexible PEG chains.

#### 3. Results and Discussion

## 3.1. Energy transport in molecules embedded in a solid polymer matrix.

Solvent-subtracted linear absorption vibrational spectra of azPEG4 in CCl<sub>4</sub>, CDCl<sub>3</sub>, and DMSO solutions and in polystyrene film are shown in Figure 1B. The strongest peak at ~1740 cm<sup>-1</sup> is due to antisymmetric C=O stretching motion of two carbonyl groups of the succinimide moiety,  $v_{\text{C=O}}$ ,  $^{38}$  and the peak at ca. 2100 cm<sup>-1</sup> is due to a NN stretching mode of the azido moiety,  $v_{\text{NN}}$ . These two modes were used mostly in the RA 2DIR studies reported here. A characteristic bathochromic shift of  $v_{\text{C=O}}$  in more polar solvents indicates that the carbonyl groups of the succinimide moiety are polarized and accessible to solvation. The solvatochromic shifts are much smaller for the azido group, indicating its smaller polarization.

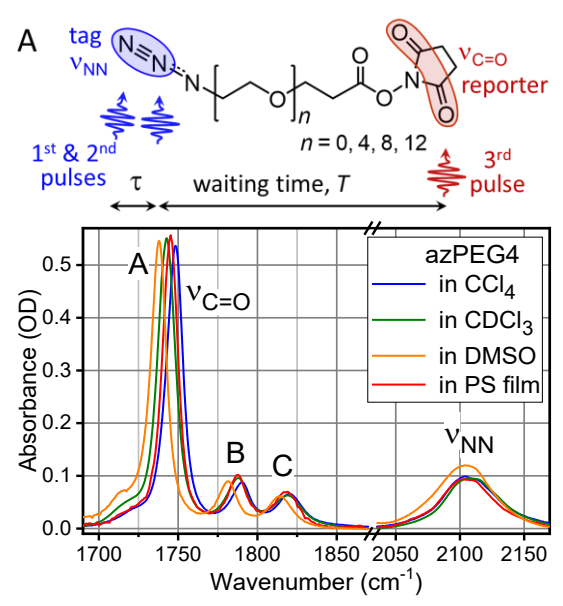


**Fig. 1. A.** Molecular structure of azPEG*n* compounds. Time delays between the mid-IR pulses used in 2DIR experiments are shown. **B.** Linear absorption spectra of azPEG4 in CCl<sub>4</sub>, CDCl<sub>3</sub>, and DMSO solutions and in a polystyrene film.

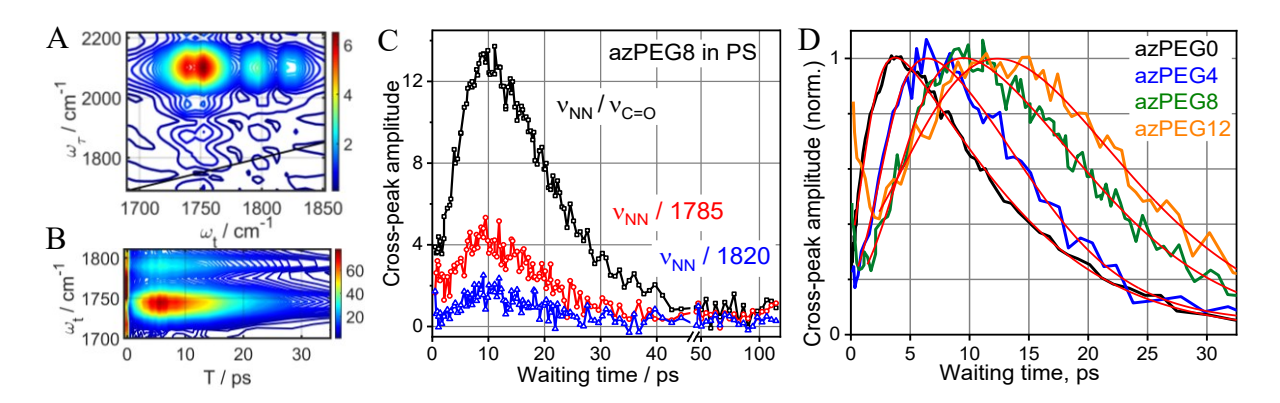


**Fig. 2. A.** 2DIR magnitude spectrum of azPEG4 in PS at T=3 ps, showing the cross peaks between  $v_{NN}$  at  $ω_τ=2100$  cm<sup>-1</sup> and  $v_{C=0}$  at  $ω_t=1740$  cm<sup>-1</sup> and two additional cross peaks are seen between  $v_{NN}$  and two other carbonyl modes at 1785 and 1820 cm<sup>-1</sup>. **B.** Waiting time dependence of the  $v_{NN}/v_{C=0}$  cross peak for azPEG4 in PS. **C.** Waiting time dependences of the three cross-peaks for azPEG8 in PS. **D.** Waiting time dependences of the  $v_{NN}/v_{C=0}$  cross-peak amplitude for the four indicated compounds in PS.

Figure 2A shows an example of a 2DIR spectrum of azPEG4 in PS featuring three cross peaks between  $v_{NN}$  at  $\omega_{\tau}$  =2100 cm<sup>-1</sup> and three carbonyl modes at  $\omega_t$  of 1740 cm<sup>-1</sup> ( $v_{C=0}$ ), 1785 and 1820 cm<sup>-1</sup>. Panel B shows how the  $v_{NN}/v_{C=0}$  cross peak amplitude changes with the waiting time. A maximum observed at ca. 6 ps is due to a relaxation-assisted 2DIR contribution – arrival of the excess energy from  $v_{NN}$  to the reporter site. 10 Integration within the  $\omega_t$  window around each peak results in one-dimensional Tdelay traces shown in panels C and D. Panel C shows that the traces for all three cross peaks behave similarly, with some differences discussed previously.<sup>17</sup> The waiting-time traces for the  $v_{NN}/v_{C=0}$  cross peak for four compounds with different chain lengths are shown in panel D. At small waiting times (T < 1 ps), when the v<sub>NN</sub> mode is still excited, the cross peak originates from the direct coupling of the v<sub>NN</sub> and v<sub>C=O</sub> oscillators. Such coupling is small because of a large distance between N<sub>3</sub> and CO groups in all these compounds. Note that a non-resonant signal contribution dominates at  $T \sim 0$ . As  $v_{NN}$  relaxes to other modes, the excess energy starts propagating inside the molecule and after some time reaches the C=O site – the succinimide end group. By vibrationally exciting low-frequency modes, X, at the C=O site, the v<sub>C=0</sub> mode frequency became affected, as the C=0 transition now involves a combination band of X + C=O, which is shifted from the vx+vc=o value due to X/C=O interaction. Such C=O frequency shift, induced by the arrived excess energy, results in an increase of the v<sub>NN</sub>/v<sub>C=O</sub> cross peak amplitude, as apparent in each trace in Figure 2B,C&D. The time at which the maximum occurs,  $T_{\text{max}}$ , characterizes the maximum energy arrival to the reporter site and is referred to as the energy transport time between the excited tag (v<sub>NN</sub>) and the reporter site (v<sub>C=O</sub>). As expected, it takes more time for the excess energy to pass a longer chain  $-T_{\text{max}}$  increases for longer chains. The waiting-time traces were fitted with an asymmetric double sigmoidal peak function in Origin software (red lines in Fig. 2D) and the  $T_{\text{max}}$  values were determined from the fit.

Figure 3 shows the dependence of  $T_{\text{max}}$  on the tag-reporter distance for the four azPEGn compounds in PS (blue circles). The dependence can be fitted well with a linear function, indicating that the transport occurs with a constant speed. Note that the PEG chain length is the only variable parameter in the series of studied compounds, so the difference in  $T_{\text{max}}$  values reflects different times to pass different chain lengths. The through-bond tag-reporter distances were used (see Section 2.3).

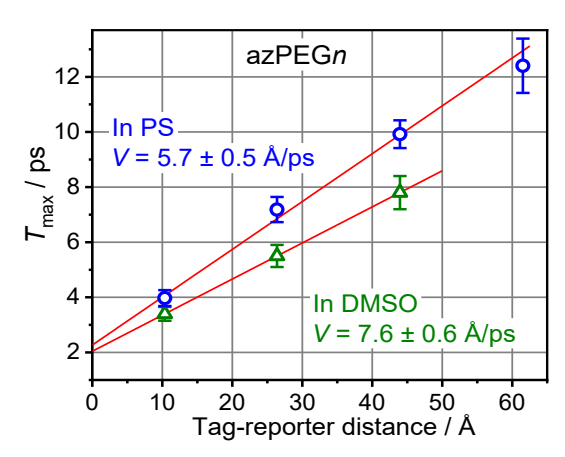


**Fig. 3.**  $T_{\text{max}}$  vs. distance for the  $v_{\text{NN}}/v_{\text{C=O}}$  cross peak for azPEGn compounds in PS (blue, n = 0, 4, 8, 12) and DMSO (green, n = 0, 4, 8). Linear fits (red lines) and resulting transport speeds are shown.

An inverse slope of the dependence in Figure 3 equals to the through-chain transport speed, determined at  $5.7 \pm 0.5$  Å/ps in the PS matrix. This speed is similar to the speed reported for the PEG chains in deuterated chloroform  $(5.3 \pm 0.4 \text{ Å/ps})^{16}$  but somewhat higher than that in CCl<sub>4</sub>  $(4.6 \pm 0.4 \text{ Å/ps})^{17}$  The speed similarity suggests that dynamic fluctuations, occurring in solution but largely frozen in the solid matrix, are not the dominant cause of the dephasing of the chain states in these non-polar solvents, nor in PS.

## 3.2. Energy transport in azPEGn dissolved in polar solvents.

To investigate how the polar environments affect the intramolecular energy transport, the  $v_{NN}/v_{C=O}$  cross-peak measurements were performed with azPEGn dissolved in more polar solvents, such as THF, methanol, and DMSO. Interestingly, the  $T_{max}$  values measured for the azPEG8 compound in more polar media are smaller than those in nonpolar media, including PS (Figure 4A, blue circles), and the reduction is substantial at 2-4 ps. Note that the end-to-end energy transport involves several distinct stages, including the tag lifetime, through-chain transport, and the transport from the chain end deeper into the succinimide moiety, bearing the reporter,  $v_{C=O}$  (Scheme 1). Each of these stages can be affected by the solvent, changing the  $T_{max}$  values.

The  $v_{NN}$  lifetime in azPEGn compounds is ca. 1 ps and depends weakly on the solvent. For example, the  $v_{NN}$  lifetime for N<sub>3</sub>-(CH2)<sub>11</sub>-CN compound varies by less than 0.1 ps when the solvent is changed from nonpolar hexane ( $\epsilon$  = 1.88; lifetime of 0.81  $\pm$  0.4 ps) and ethyl acetate ( $\epsilon$  = 6.0, lifetime of 0.77  $\pm$  0.4 ps) to polar propanol ( $\epsilon$  = 20.1, lifetime of 0.73  $\pm$  0.5 ps).<sup>39</sup> Therefore, only a small contribution to the observed  $T_{max}$  changes is expected from the  $v_{NN}$  lifetime shortening in polar solvents.

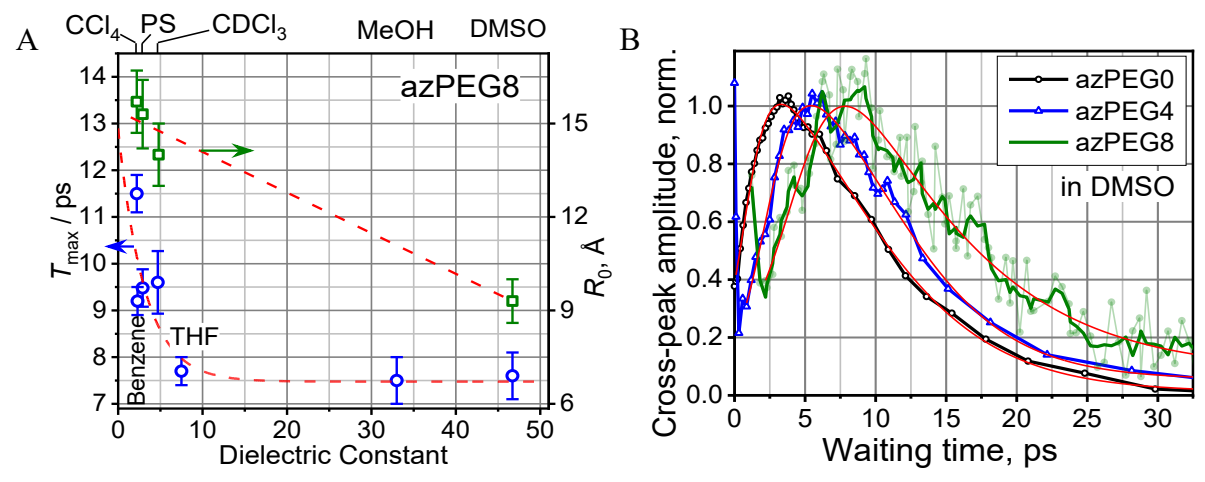
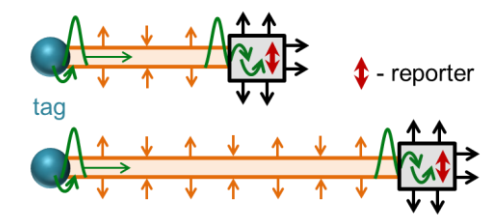


**Fig. 4. A.** Dependence of  $T_{\text{max}}$  (blue circles, left axis) and of spatial exponential decay factor,  $R_0$ , (green squares, right axis) on the dielectric constant (ε) of the medium for the  $v_{\text{NN}}$  /  $v_{\text{C=O}}$  cross peak for azPEG8. To avoid crowding, the points for PS are shown at ε=2.9 instead of the actual value of ε=2.6 for PS. Dashed red lines provide an eye guide. **B.** Waiting time dependences of the  $v_{\text{NN}}$  /  $v_{\text{C=O}}$  cross peak amplitude for azPEGn in DMSO.



**Scheme 1.** Cartoon describing ballistic energy propagation and energy losses to the solvent in two molecules featuring different chain lengths. The wavepacket generated in the chain, shown as a green peak, propagates within the chain (orange rectangle) and reaches the end group (black box), which bears the reporter (red). Energy losses at the end group are shown with black arrows. Orange arrows reflect dephasing and relaxation of the chain states.

The last stage of the transport, diffusive steps within the end group towards the reporter, is expected to become faster in more polar solvents. Stronger interaction with the solvent results in larger state energy fluctuations, thus offering more efficient intramolecular vibrational redistribution (IVR) channels within the solute. A faster end-group transport steps were recently observed of azPEGn in PS at elevated temperatures.<sup>37</sup> A quantitative assessment of this effect was difficult with the available data.

To investigate how the through-chain transport is affected by the solvent polarity, the RA 2DIR measurements were performed in DMSO for three compounds with 0, 4, and 8 PEG units. Note that the cross-peak signals for azPEG12 were too weak to measure. The waiting time dependences are shown in Figure 4B. The dependence of  $T_{\text{max}}$  on the tag-reporter distance is shown in Figure 3 (green triangles). Apparently, the through-chain transport speed in DMSO (7.6  $\pm$  0.6 Å/ps) is faster than that in PS by ca. 1.4 fold. The result is counterintuitive as stronger interaction within a more polar solvent is expected to increase the dephasing of the chain states.<sup>37</sup> The chain states dephasing breaks the wavepacket and eventually results in energy dissipation within in the chain, thus delivering negligible amount of energy to the reporter site. Thus, if changed at all, a slower transport speed is expected in more polar solvents. Note that the number of wavepackets reached the end group without being dephased, decreases exponentially with the chain length, resulting in a reduction of the cross-peak amplitude with the chain length.<sup>23</sup> However, per molecule, the amount of energy delivered to the end group is constant, defined by

the energies of the chain-band states transferring the wavepacket. Because the same amount of energy is delivered to the end group (Scheme 1, green peak), the relaxation processes at the end group are expected to be independent of the chain length (Scheme 1, black arrows).

The transport efficiency is an important characteristic of the transport. The  $v_{NN}/v_{C=0}$  cross peak amplitude was measured for the azPEGn samples featuring the same concentrations (same IR peak absorptions). Figure 5 shows the results for azPEGn in PS (blue circles) and in DMSO (green triangles). A fit to a single-exponential function,  $A \times \exp(-R/R_0)$ , was used to determine the spatial decay factor,  $R_0$ . The  $R_0$  in DMSO (9.3  $\pm$  0.7 Å) is found to be much shorter than that in PS (15.1  $\pm$  1.1 Å), indicating much larger cooling rate in DMSO. Note that these dependences emphasize the energy losses from the chain, as only the chain length is varied in the data of Figure 5.

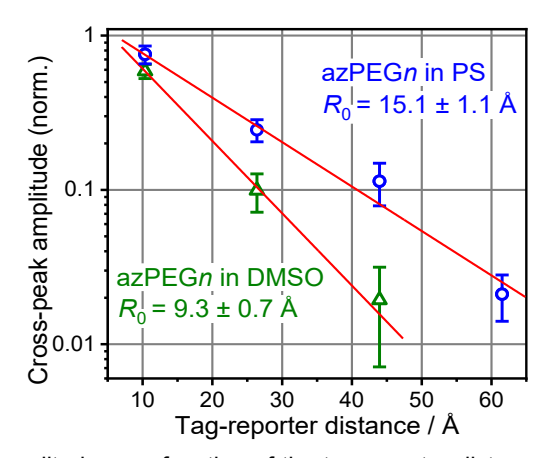


**Fig. 5. A.**  $v_{\text{NN}}/v_{\text{C=O}}$  cross peak amplitude as a function of the tag-reporter distance for the azPEG*n* compounds in a PS film (n = 0, 4, 8, 12, blue circles) and in DMSO solution (n = 0, 4, 8, 9 green triangles). Single-exponential fits resulted in  $R_0$  decay factors of 15.1  $\pm$  1.1 Å in PS and 9.3  $\pm$  0.7 Å in DMSO.

To understand the origin of the speed change, we compared the decay (cooling) portions for the waiting-time traces for different media measured for the same compounds, azPEG0 and azPEG4 (Fig. 6). The decay times obtained via a single exponential fit of the decay tails starting at ca. 70% level from the maximum, correlate with the solvent polarity. For example, the decay time for azPEG4 in DMSO is ca. 1.3 times shorter than that in CCl4 (see the decay times in the insets). Naturally, the solute-medium interaction strength increases with an increase in the medium polarity, resulting in a faster cooling. Note that the  $T_{\rm max}$  values depend on the relaxation processes at the end group – if no cooling occurs at the end group, the maximum signal would be found at infinite waiting time. The use of  $T_{\rm max}$  values for assessing the energy transport times is convenient from the experimental point of view, as it allows to avoid the non-resonant signal contribution at small waiting times, a plateau contribution at large waiting times and it can be easily and uniquely determined. Note also that a double-exponential function is not representing well the shapes of the waiting-time traces and obtaining the exponential times for such shapes is an ill-defined problem.

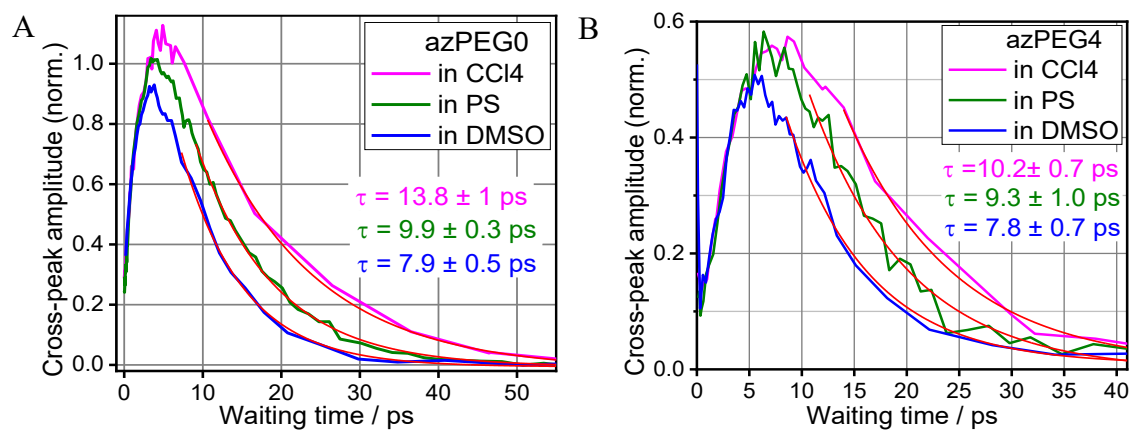


**Fig. 6.** Waiting time dependences of the  $v_{NN}$  /  $v_{C=0}$  cross peak amplitude for (A) azPEG0 and (B) azPEG4 in CCl<sub>4</sub> (magenta), PS (green), and DMSO (blue). The traces are normalized to maximize an overlap of the rising part of the curves. Fits with a single exponential function for the decaying portion of the traces are shown with red lines; the resulting decay times are given in the insets.

The effect of the end-group relaxation on the  $T_{\rm max}$  values can be clearly seen by comparing the waiting time traces for the same compound in the solvents of different polarity (Fig. 6). The traces in both panels are normalized in such a way that the rising portions of the traces overlap the most; although the overlap is not ideal, the rising parts of the traces are indeed similar for all three solvents both compounds, azPEG0 (Fig. 6A) and azPEG4 (Fig. 6B), confirming that a similar energy quantum is delivered to the end group in each solvent. The maximum ( $T_{\rm max}$ ) is dependent on the cooling rate at the end group, shifting to larger values when the rate decreases.

The comparison of the traces for different compounds in the same solvent revealed that the traces do not overlap by just a shift to longer delays for longer chains but have shape differences. For example, the apparent cooling time changes with the chain length, becoming shorter for longer chains. The rising potion of the traces is not precisely the same for different chain length either, as easy to see from Figures 2D and 4B. As the traces feature different shapes, the transport speed determination from them is not unique. For example, the speed determined using half-rise times is faster than that determined from  $T_{\text{max}}$ , as apparent from smaller increments to the transport time at the half-rise time for every longer compound (Fig. 2D, 4B). However, the signals at small waiting times are polluted by the non-resonant and partially resonant contributions, apparent with spikes at small T (Figures 2D, 4B, and 6), which introduces errors in speed determination.

A 0.8-fraction level from the maximum was selected for the speed evaluation,  $T_{0.8}$ , which permits avoiding significantly the non-resonant contributions and reduces greatly the influence of unequal cooling. At the same time, the 0.8 level reflects the arrival of the majority of the excess energy, not just signaling via the fastest wavepacket that does not deliver much of the excess energy.

The  $T_{0.8}$  values for the azPEGn in PS and DMSO appear to be more similar for all chain lengths (Fig. 7), resulting in similar transport speeds of  $9.2 \pm 0.5$  Å/ps and  $9.7 \pm 0.3$  Å/ps, respectively. The speed determined with  $T_{0.8}$  is significantly higher than that for  $T_{\text{max}}$  and the difference in speeds in PS and DMSO became small. Note that the  $T_{0.8}$  values do not completely eliminate the dependence on the end-group cooling rate but reduces it greatly.

However, even with  $T_{0.8}$  approach, the speed in CCl<sub>4</sub>,<sup>17</sup> featuring the weakest solute-solvent interaction, appears to be significantly lower than that in PS and DMSO (Fig. 7, black squares). Different speeds can be explained assuming that there are several wavepackets contributing to the transport, featuring different transport speeds. Under the conditions of higher chain-state dephasing in high-polarity solvents, only the wavepacket with the faster speed survives and delivers energy to the end group, as it spends less time within the chain. With smaller dephasing rates in non-polar solvents, both wavepackets

contribute, resulting in an average speed, which is smaller than that of the fastest wavepacket, as illustrated in Scheme 2.

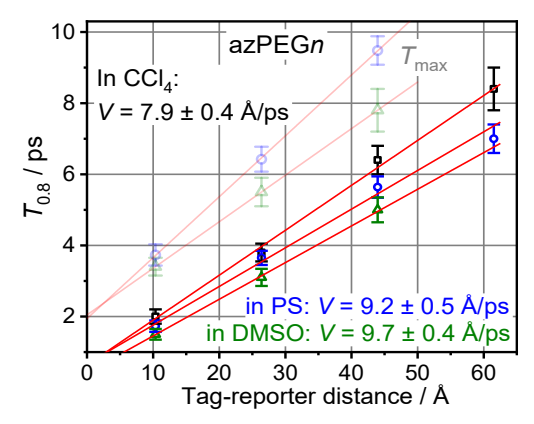
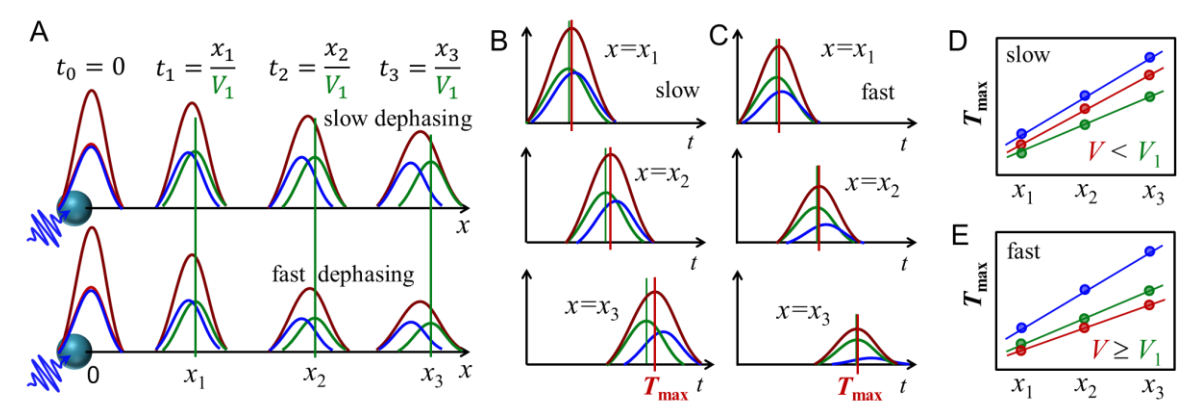


**Fig. 7.**  $T_{0.8}$  vs. distance for  $v_{NN}/v_{C=0}$  cross peak of azPEGn compounds in PS (blue), DMSO (green), an CCl<sub>4</sub> (black). Linear fits (red lines) and resulting transport speeds are shown. The light-colored data show  $T_{max}$  vs. distance dependence (taken from Fig. 3) in PS and DMSO for comparison.



**Scheme 2.** Cartoon showing how the measured speed can change if two wavepackets with different group velocities propagate at the same time in the medium with slow (A-top, B, D) dephasing and fast (A-bottom, C, and E) chain-state dephasing. Panel A shows snapshots of positions in space of two wavepackets: the 1<sup>st</sup> one (green) propagates with velocity  $V_1$  and the 2<sup>nd</sup> (blue) moves slower. The locations of both wavepacket are recorded at time delays when the 1<sup>st</sup> wavepacket reaches distances 0,  $x_1$ ,  $x_2$ , and  $x_3$  from the tag. Panels B and C show the excess-energy time profiles at the coordinates  $x_1$ ,  $x_2$ , and  $x_3$  due to each wavepacket and for overall energy (red) for slow (B) and fast (C) dephasing. The green and red vertical lines indicate the delay time when the maximum is achieved for the 1<sup>st</sup> wavepacket (green) and for the overall energy (red). The  $T_{max}$  values are shown in panel D for the slow (top) and fast (bottom) dephasing. The points for individual wavepackets (blue and green) are the same on both graphs, while the  $T_{max}$  values for the overall energy arrival (red) are changing, depending on the dephasing rate. Considering both wavepackets together, the transport speed is slower than  $V_1$  for the slow dephasing case (top) and slightly faster than  $V_1$  for the fast dephasing case.

# **Concluding remarks**

RA 2DIR spectroscopy provides a powerful tool to study intramolecular energy transport. Interactions with the solvent affect the energy transport within the molecule. The similarity of the transport times in a polymer matrix and solution of similar polarity suggests that dynamic fluctuations of the media, occurring in solution but largely frozen in a solid matrix, are not the dominant cause of the chain state dephasing, despite the presence of fast relaxation components for the solvents. The through-chain transport efficiency is significantly reduced in more polar solvents as the chain-state dephasing rate increases with an increase of the solute-solvent interaction strength. As reported previously, the transport

in nonpolar solvents occurs ballistically only to distances of ca. 6-8 PEG units, switching to directed diffusion regime at longer distances.<sup>41</sup> The directed diffusion regime occurs with a similar speed to the ballistic transport and similarly relies on the dephasing of the chain states.<sup>23</sup> An increased chain-state dephasing in DMSO, apparent from the decreased transport efficiency, likely results in a switch to the directed diffusive regime at shorter chain lengths, compared to that in nonpolar solvents. The end-group energy dissipation rate, the cooling rate, is found to correlate with the dielectric constant of the solvent or matrix. The waiting time dependences for the end-group-to-end-group cross peak amplitude are compared for the molecules dissolved in different solvents, revealing that the cooling process of the reporter end-group affects the  $T_{\text{max}}$  values significantly, thus affecting the apparent through-chain transport speed. Moreover, the shape of the waiting-time dependence changes with the chain length, eliminating a unique way of defining the transport speed. We found that by using the  $T_{0.8}$  times, instead of  $T_{\text{max}}$ , the majority of the dependence on the end-group cooling rate is eliminated. The transport speed resulted from T<sub>0.8</sub> values for different chain lengths still shows some dependence on the solvent polarity. Such dependence is explained by the existence of multiple wavepackets featuring different group velocities, propagating either together in the same molecule or in different molecules of the sample. Collectively, these wavepackets spread the arrival time to the reporter site over some time interval. In the media with small losses, more than one wavepacket can survive and deliver energy to the end group, resulting in a transport speed, that is an average of the speeds for different wavepackets. In the media with higher losses, such as DMSO, only the fastest wavepacket survives, so the observed speed matches the speed of the fastest wavepacket. The study reveals intimate details of the ballistic energy transport in PEG oligomers via optical chain bands, which can help selecting the environment to ensure most efficient energy transport to larger distances.

## Acknowledgement

The study is supported by the NSF CHE-1900568 grant and the Tulane University Bridge Fund.

#### References

- 1. Fermi, E.; Pasta, J.; Ulam, S., Studies of the Nonlinear Problems. *Los Alamos Report* **1955**, LA-1940.
- 2. Logan, D. E.; Wolynes, P. G., Quantum localization and energy flow in many-dimensional Fermi resonant systems. *J. Chem. Phys.* **1990**, *93*, 4994.
- 3. Davydov, A. S., Solitons and Energy Transfer Along Protein Molecules. *J. Theor. Biol.* **1977**, *66*, 379-387.
- 4. Backus, E. H. G.; Nguyen, P. H.; Botan, V.; Pfister, R.; Moretto, A.; Crisma, M.; Toniolo, C.; Stock, G.; Hamm, P., Energy Transport in Peptide Helices: A Comparison between Highand Low-Energy excitation. *J. Phys. Chem.* **2008**, *112*, 9091-9099.
- 5. Schwarzer, D.; Hanisch, C.; Kutne, P.; Troe, J., Vibrational Energy Transfer in Highly Excited Bridged Azulene-Aryl Compounds: Direct Observation of Energy Flow through Aliphatic Chains and into the Solvent. *J. Phys. Chem. A* **2002**, *106* (35), 8019-8028.
- 6. Schwarzer, D.; Kutne, P.; Schroeder, C.; Troe, J., Intramolecular vibrational energy redistribution in bridged azulene-anthracene compounds: Ballistic energy transport through molecular chains. *J. Chem. Phys.* **2004**, *121* (4), 1754-1764.
- 7. Wang, Z.; Carter, J. A.; Lagutchev, A.; Koh, Y. K.; Seong, N.-H.; Cahill, D. G.; Dlott, D. D., Ultrafast flash thermal conductance of molecular chains. *Science* **2007**, *317*, 787-790.
- 8. Hamm, P.; Lim, M.; Hochstrasser, R. M., Structure of the amide I band of peptides measured by femtosecond non-linear infrared spectroscopy. *J. Phys. Chem. B* **1998**, *102* (31), 6123-6138.

- 9. Asplund, M. C.; Zanni, M. T.; Hochstrasser, R. M., Two-dimensional infrared spectroscopy of peptides by phase-controlled femtosecond vibrational photon echoes. *Proc. Natl. Acad. Sci. U.S.A.* **2000,** *97* (15), 8219-8224.
- 10. Rubtsova, N. I.; Rubtsov, I. V., Vibrational energy transport in molecules studied by relaxation-assisted two-dimensional infrared spectroscopy. *Ann. Rev. Phys. Chem.* **2015**, *66*, 717-738.
- 11. Schmitz, A. J.; Pandey, H. D.; Chalyavi, F.; Shi, T.; Fenlon, E. E.; Brewer, S. H.; Leitner, D. M.; Tucker, M. J., Tuning Molecular Vibrational Energy Flow within an Aromatic Scaffold via Anharmonic Coupling. *J. Phys. Chem. A* **2019**, *123* (49), 10571-10581.
- 12. Müller-Werkmeister, H. M.; Li, Y.-L.; Lerch, E.-B. W.; Bigourd, D.; Bredenbeck, J., Ultrafast Hopping from Band to Band: Assigning Infrared Spectra based on Vibrational Energy Transfer. *Angew. Chemie Intern. Ed.* **2013**, *52* (24), 6214-6217.
- 13. Schade, M.; Moretto, A.; Crisma, M.; Toniolo, C.; Hamm, P., Vibrational energy transport in peptide helices after excitation of C-D modes in Leu-d10. *J. Phys. Chem. B* **2009**, *113* (40), 13393-13397.
- 14. Rubtsov, I. V.; Wang, J.; Hochstrasser, R. M., Dual frequency 2D-IR heterodyned photon-echo of the peptide bond. *Proc. Natl. Acad. Sci. U.S.A.* **2003**, *100* (10), 5601-5606.
- 15. Kurochkin, D. V.; Naraharisetty, S. G.; Rubtsov, I. V., Relaxation-assisted 2DIR spectroscopy method. *Proc. Natl. Acad. Sci. U.S.A.* **2007**, *104* (36), 14209-14214.
- 16. Lin, Z.; Rubtsov, I. V., Constant-speed vibrational signaling along polyethyleneglycol chain up to 60-Å distance. *Proc. Natl. Acad. Sci. U.S.A.* **2012**, *109* (5), 1413-1418.
- 17. Lin, Z.; Zhang, N.; Jayawickramarajah, J.; Rubtsov, I. V., Ballistic energy transport along PEG chains: distance dependence of the transport efficiency. *Phys. Chem. Chem. Phys.* **2012**, *14* (30), 10445-54.
- 18. Rubtsova, N. I.; Rubtsov, I. V., Ballistic energy transport via perfluoroalkane linkers. *Chem. Phys.* **2013**, *422*, 16-21.
- 19. Rubtsova, N. I.; Kurnosov, A. A.; Burin, A. L.; Rubtsov, I. V., Temperature dependence of the ballistic energy transport in perfluoroalkanes. *J. Phys. Chem. B* **2014**, *118* (28), 8381-8387.
- 20. Rubtsova, N. I.; Nyby, C. M.; Zhang, H.; Zhang, B.; Zhou, X.; Jayawickramarajah, J.; Burin, A. L.; Rubtsov, I. V., Room-temperature ballistic energy transport in molecules with repeating units *J. Chem. Phys.* **2015**, *142*, 212412.
- 21. Yue, Y.; Qasim, L. N.; Kurnosov, A. A.; Rubtsova, N. I.; Mackin, R. T.; Zhang, H.; Zhang, B.; Zhou, X.; Jayawickramarajah, J.; Burin, A. L.; Rubtsov, I. V., Band-selective ballistic energy transport in alkane oligomers: toward controlling the transport speed. *J. Phys. Chem. B* **2015**, *119* (21), 6448-56.
- 22. Qasim, L. N.; Atuk, E. B.; Maksymov, A. O.; Jayawickramarajah, J.; Burin, A. L.; Rubtsov, I. V., Ballistic Transport of Vibrational Energy through an Amide Group Bridging Alkyl Chains. *J. Phys. Chem. C* **2019**, *123*, 3381-3392.
- 23. Kurnosov, A. A.; Rubtsov, I. V.; Burin, A. L., Fast transport and relaxation of vibrational energy in polymer chains. *J. Chem. Phys.* **2015**, *142* (1), 011101.
- 24. Segal, D.; Nitzan, A.; Hanggi, P., Thermal conductance through molecular wires. *J. Chem. Phys.* **2003**, *119* (13), 6840-6855.
- 25. Burin, A. L.; Tesar, S. L.; Kasyanenko, V. M.; Rubtsov, I. V.; Rubtsov, G. I., Semiclassical model for vibrational dynamics of polyatomic molecules: Investigation of Internal Vibrational Relaxation. *J. Phys. Chem. C* **2010**, *114* (48), 20510-20517.

- 26. Tesar, S. L.; Kasyanenko, V. M.; Rubtsov, I. V.; Rubtsov, G. I.; Burin, A. L., Theoretical study of internal vibrational relaxation and energy transport in polyatomic molecules. *J. Phys. Chem. A* **2013**, *117* (2), 315-323.
- 27. Benderskii, V. A.; Kats, E. I., Propagating vibrational excitations in molecular chains. *JETP Lett.* **2011,** *94*, 459-464.
- 28. Leitner, D. M., Thermal Boundary Conductance and Thermal Rectification in Molecules. *J. Phys. Chem. B* **2013**, *117* 12820-12828.
- 29. Benderskii, V. A.; Kotkin, A. S.; Rubtsov, I. V.; Kats, E. I., Vibrational energy transport in molecular wires *JETP Letters* **2013**, *98* (4), 219-222.
- 30. Leitner, D. M., Quantum ergodicity and energy flow in molecules. *Advances in Physics* **2015**, *64*, 445.
- 31. Fujisaki, H.; Yagi, K.; Kikuchi, H.; Takami, T.; Stock, G., Vibrational energy transport in acetylbenzonitrile described by an ab initio-based quantum tier model. *Chem. Phys.* **2017**, 482, 86-92.
- 32. Pandey, H. D.; Leitner, D. M., Influence of thermalization on thermal conduction through molecular junctions: Computational study of PEG oligomers. *J. Chem. Phys.* **2017**, *147* (8), 084701.
- 33. Naraharisetty, S. G.; Kasyanenko, V. M.; Rubtsov, I. V., Bond connectivity measured via relaxation-assisted two-dimensional infrared spectroscopy. *J. Chem. Phys.* **2008**, *128*, 104502.
- 34. Leger, J. D.; Nyby, C. M.; Varner, C.; Tang, J.; Rubtsova, N. I.; Yue, Y.; Kireev, V. V.; Burtsev, V. D.; Qasim, L. N.; Rubtsov, G. I.; Rubtsov, I. V., Fully automated dual-frequency three-pulse-echo 2DIR spectrometer accessing spectral range from 800 to 4000 wavenumbers. *Rev. Sci. Instrum.* **2014**, *85* (8), 083109.
- 35. Nyby, C. M.; Leger, J. D.; Tang, J.; Varner, C.; Kireev, V. V.; Rubtsov, I. V., Mid-IR beam direction stabilization scheme for vibrational spectroscopy, including dual-frequency 2DIR. *Opt. Express* **2014**, *22* (6), 6801-9.
- 36. Hamm, P.; Zanni, M. T., *Concepts and methods of 2D infrared spectroscopy*. 1st ed.; Cambridge University Pres: Cambridge; New York, 2011; p ix, 286 p.
- 37. Mackin, R. T.; Leong, T. X.; Rubtsova, N. I.; Burin, A. L.; Rubtsov, I. V., Low-Temperature Vibrational Energy Transport via PEG Chains. *J. Phys. Chem. Lett.* **2020**, *11* (12), 4578-4583.
- 38. Lin, Z.; Keiffer, P.; Rubtsov, I. V., Method for determining small anharmonicity values from 2DIR spectra using thermally induced shifts of frequencies of high-frequency modes. *J. Phys. Chem. B* **2011**, *115* (18), 5347-5353.
- 39. Varner, C.; Zhou, X.; Saxman, Z. K.; Leger, J. D.; Jayawickramarajah, J.; Rubtsov, I. V., Azido alkanes as convenient reporters for mobility within lipid membranes. *Chem. Phys.* **2018**, *512*, 20-26.
- 40. Horng, M. L.; Gardecki, J. A.; Papazyan, A.; Maroncelli, M., Subpicosecond Measurements of Polar Solvation Dynamics Coumarin-153 Revisited. *J. Phys. Chem.* **1995**, *99* (48), 17311-17337.
- 41. Qasim, L. N.; Kurnosov, A. A.; Yue, Y.; Lin, Z.; Burin, A. L.; Rubtsov, I. V., Energy transport in PEG oligomers: Contributions of different optical bands. *J. Phys. Chem. C.* **2016**, 120 (47), 26663.